USAARL Report No. 2020-02

Constructing a One-Piece Integrated Tissue Scaffold for a Biofidelic Eye Model

By Michael K. Smolek, Morris R. Lattimore,
Thomas H. Harding, James Q. Truong

United States Army Aeromedical Research Laboratory

Warfighter Performance Group

December 2019

Notice

Qualified Requesters

Qualified requesters may obtain copies from the Defense Technical Information Center (DTIC), Fort Belvoir, Virginia 22060. Orders will be expedited if placed through the librarian or other person designated to request documents from DTIC.

Change of Address

Organizations receiving reports from the U.S. Army Aeromedical Research Laboratory on automatic mailing lists should confirm correct address when corresponding about laboratory reports.

Disposition

Destroy this document when it is no longer needed. Do not return it to the originator.

Disclaimer

The views, opinions, and/or findings contained in this report are those of the author(s) and should not be construed as an official Department of the Army position, policy, or decision, unless so designated by other official documentation. Citation of trade names in this report does not constitute an official Department of the Army endorsement or approval of the use of such commercial items.

REPORT DOCUMENTATION PAGE

Form Approved
OMB No. 0704-0188

1. REPORT DATE *(DD-MM-YYYY)*	2. REPORT TYPE	3. DATES COVERED *(From - To)*
17-12-2019	Technical Report	

4. TITLE AND SUBTITLE

Constructing a One-Piece Integrated Tissue Scaffold for a Biofidelic Eye Model

5a. CONTRACT NUMBER

5b. GRANT NUMBER

5c. PROGRAM ELEMENT NUMBER

6. AUTHOR(S)

Smolek, Michael K.; Lattimore, Morris R.; Harding, Thomas H.; Truong James Q.

5d. PROJECT NUMBER

5e. TASK NUMBER

5f. WORK UNIT NUMBER

7. PERFORMING ORGANIZATION NAME(S) AND ADDRESS(ES)

U.S. Army Aeromedical Research Laboratory
P.O. Box 620577
Fort Rucker, AL 36362

8. PERFORMING ORGANIZATION REPORT NUMBER

USAARL 2020-02

9. SPONSORING/MONITORING AGENCY NAME(S) AND ADDRESS(ES)

U.S. Army Aeromedical Research Laboratory
P.O. Box 620577
Fort Rucker, AL 36362

10. SPONSOR/MONITOR'S ACRONYM(S)

11. SPONSOR/MONITOR'S REPORT NUMBER(S)

12. DISTRIBUTION/AVAILABILITY STATEMENT

Approved for public release; Distribution unlimited.

13. SUPPLEMENTARY NOTES

14. ABSTRACT

Primary blast injuries (PBIs) caused by shock waves traveling within the human eye and orbit are not fully understood. Collecting intraocular biomechanical response data from postmortem eyes is challenging, and laboratory animal data are difficult to translate into human outcomes because of anatomical differences. Here, we show a bioengineered, fluid-filled model of the corneoscleral shell of the human eye designed to allow rigorous, highly repeatable studies of both ocular PBI outcomes and the efficacy of blast protection eyewear designs. The model is cast as a one-piece, structurally integrated, alginate-based hydrogel scaffold that has adjustable tensile strength through synthetic or biological hybridization. The model can be pre-stressed to a physiological intraocular pressure, embedded with living cells for investigating trauma pathology, and instrumented with fiber-optic sensors for recording overpressure data during blast testing. Correlating the overpressure at key intraocular locations with the cellular expression of molecular biomarkers for trauma will be helpful in predicting the risk for vision loss. This model has other applications, including the creation of corneal graft tissue and enabling surgical simulations for training.

15. SUBJECT TERMS

Biomedical, Materials and Manufacturing Processes, Anatomy and Physiology, Manufacturing Technology for Affordability

16. SECURITY CLASSIFICATION OF:			17. LIMITATION OF ABSTRACT	18. NUMBER OF PAGES	19a. NAME OF RESPONSIBLE PERSON
a. REPORT	b. ABSTRACT	c. THIS PAGE			Loraine St. Onge, PhD
UNCLAS	UNCLAS	UNCLAS	SAR	30	19b. TELEPHONE NUMBER *(Include area code)* 334-255-6906

This page is intentionally blank.

Table of Contents

List of Tables

List of Figures

This page is intentionally blank.

Introduction

Primary blast injury (PBI) occurs when a supersonic shock wave (i.e., overpressure) interacts destructively with the tissues of the body, resulting in one or more forms of physical trauma (Garner & Brett, 2007; Smith & Garner, 2019; Wightman & Gladish, 2001). It is assumed that overpressure induces compression or shearing stresses that cause the strain limit of the impacted tissue to be exceeded. Because different tissues can have different strain limits, and the pattern of overpressure can vary with blast parameters, controlled experiments of PBI have been inherently difficult to perform. Primary blast injury (PBI) may include trauma to the lungs, traumatic brain injury (TBI), complete or partial loss of hearing, and/or a complete or partial loss of vision (Beamer et al., 2016; Beiran & Miller, 1992; Chalioulias, Sim, & Scott, 2007; Lo et al., 2013; Petras, Bauman, & Elsayed, 1997; Scott et al., 2017; Van Haesendonck, Van Rompaey, Gilles, Topsakal, & Van de Heyning, 2018).

While trauma from a shrapnel impact is often obvious, PBI is likely to be an occult trauma that is undiagnosed at the time of the blast event (Smith & Garner, 2019; Wightman & Gladish, 2001). A confirmed diagnosis of PBI may come weeks or months after the initial trauma, and in some cases, a diagnosis of PBI might not be confirmed unless an autopsy is conducted. Often PBI becomes manifest through clinical testing only after unexplained sensory deficits or behavioral changes related to neurological dysfunction are reported by the victim or family members. Ocular PBI, for example, may be suspected when a blast victim notices a chronic change in optical clarity, color vision, double vision, or areas of lost vision in one or both eyes (Chalioulias et al., 2007). According to a review of the Joint Theater Trauma Registry (JTTR) for data recorded between 2002 to 2011, explosive blasts caused 92 percent (%) of ocular injuries sustained in combat, with approximately half of the injuries attributed to PBI (Lo et al., 2013). While ocular PBI has received less attention than TBI, a growing body of scientific and clinical evidence confirms that shock waves propagating within the eye and ocular orbit can cause overpressure-induced injuries, affecting one or more physiological or neurological functions resulting in vision loss (Beiran & Miller, 1992; Chalioulias et al., 2007; Lo et al., 2013; Petras et al., 1997; Sherwood et al., 2014).

Translating ocular PBI data that have been acquired from experimental animal models into a predictable visual loss in humans is challenging because the predominant models, namely rodents and pigs, have eyes and skulls that are morphologically dissimilar to humans. Therefore, any evidence of overpressure-induced trauma obtained with animal models may poorly correlate to trauma in the human eye for the same shock wave parameters. Likewise, predicting the relative severity of overpressure trauma is problematic because of physical scaling differences when comparing the anatomy of humans and small laboratory animals (Hubbard, Hall, Siva Sai Suijith Sajja, Lavik, & VandeVord, 2014; Turner et al., 2013). Furthermore, animal models cannot be used to test and evaluate the efficacy of protective eyewear made to fit the human head. Although non-human primates are more anatomically similar to humans, they have not been widely used as an ocular PBI model, most likely due to the cost involved. For now, ocular PBI predictions based on computer modeling has been of limited benefit because of the inability to validate these models experimentally. However, the acquisition of more accurate and precise empirically acquired data could substantially improve the reliability of computer simulations of ocular PBI (Bhardwaj, Ziegler, Seo, Ramesh, & Nguyen, 2014; Rigas & Sklavounos, 2005; Watson et al., 2015; Zhang, Pintar, Yoganandan, Gennarelli, & Son, 2009; Zhu et al., 2012).

Finally, overpressure data obtained from electronically instrumented headforms have little direct relevance in understanding the relationship between ocular PBI and intraorbital shock wave propagation due to a lack of anatomical correlation of bone structure between a human skull and currently manufactured headforms (Crowley, Brozoski, Duma, & Kennedy, 2009; Duma et al., 1997; Kennedy et al., 2007). A morphologically accurate physical eye model for obtaining direct measurements of blast overpressure propagation and evaluating injury biomarkers from within the eye and orbit is needed to further advance this field of research.

The surrogate human eye model would help to bridge several current research gaps. This bioengineered model has the potential to reduce the cost and regulatory oversight associated with using animals exclusively for research, and it would be useful to validate the results of computer models of blast dynamics. It would also be beneficial for evaluating the blast-resistance of existing or new types of protective eyewear. Additionally, this model contains a simulated cornea that may also have relevance for other purposes, such as modeling topographical changes in the pre-and post-blast shape of the anterior segment portion of the model. The present study describes the conceptual development and early production methods of a fluid-filled, biofidelic human eye model. Future versions of the model are planned, to include versions scaled to represent animal eyes for comparative testing, as well as versions that incorporate additional internal and external anatomical detail for improved medical simulations.

Methods

Eye Model Design Overview

The surrogate human eye model is a simulated corneoscleral shell made by a casting process in which a complete, three-dimensional (3D) structure is formed at one time as a continuous layer of hydrogel material enclosing a temporary inner core of molded gelatin that represents the anterior and posterior chambers of the eye. The inclusion of a distinct and realistic corneal shape on the model is helpful for external alignment of the model when it is mounted into a headform at a specific orientation. Additionally, a simulated optic nerve is included during casting so that its tube-like external sheath is integrated structurally with the corneoscleral globe of the eye model and extends between the eye globe and the optic canal opening at the back of the orbit. The inclusion of this simulated optic nerve is a key feature of this model because human donor eyes or excised animal eyes typically have the optic nerve severed immediately during the enucleation procedure, making them essentially useless for understanding how the optic nerve is subjected to shearing or tractional stress during a blast event. This simulated optic nerve also creates a port of entry into the model for the introduction of instrumentation via a catheter system, as well as inflation of the globe to a specific intraocular pressure (IOP) in order to place the corneoscleral shell under normal tension. This arrangement for instrumenting the eye model via the cranium reduces the likelihood that the embedded recording instrumentation will interfere with the propagation of the shock wave, and should therefore yield measurements with better accuracy.

Another important feature of the eye model is the application of an inner core of gelatin that determines the final shape of the model. This inner core also provides the necessary structural support during storage and transportation of the eye model. The inner core can remain in situ as a single piece of gelatin subject to fracturing from overpressure during blast testing, or it may be partially melted in situ to model a fully liquid aqueous humor and a semi-gelatinous vitreous humor. More often, the inner core will be removed completely in preparing the model for use, and subsequently replaced by other fluids to pressurize the globe, such as physiologically balanced saline solutions with added nutrients for perfusing the eye model, or fluids of varying viscosity to understand the effects of intraocular media density on overpressure amplitude and shock wave propagation.

Ancillary Equipment

Additional supporting equipment were included during development of the eye model, including a skull-based headform to provide a standard, anatomically accurate ocular orbit, an intraorbital eye holder to replicate soft tissues and precisely position the model, a manometer system to pressurize the eye model, and a leak-free, multi-port catheter system that allows the pressurized eye model to be instrumented with fiber optic pressure sensors or other devices that can be passed into the eye through the optic nerve sheath.

Master Models of the Inner Core

Twelve versions of the eye model's inner core (i.e., the master eye models) were made from turned birch wood. Birch wood was used for designing the initial prototype to keep the prototype development cost low. Each master eye model version had slightly different dimensions for the anterior chamber (AC) depth, diameter, and profile in order to determine the effects of the AC shape on the outcome of the corneosceral shell. Wood dowels that were approximately 100 millimeters (mm) in length were added to simulate an optic nerve on each master eye model. These dowels were inserted at an anatomically correct location and orientation with respect to the posterior pole of the master eye mode with slight variations permitted (Figure 1A). Because the prototype eye model is not specific to either the right or left eye, the insertion location of the simulated optic nerve does not take into account the small vertical offset of the true optic nerve insertion relative to the posterior pole of the globe. The acceptable mean values and standard deviations for the dimensions of the anterior and posterior chambers were obtained from published anatomical data for the adult human eye, including references to magnetic resonance imaging (MRI) of the living eye (Atchison et al., 2004; Erb-Eigner et al., 2015; Fontana & Brubaker, 1980; Gilmartin, Nagra, & Logan, 2013; Norman et al., 2010).

Silicone Master Molds

Six out of the 12 wood master eye models were selected based on their overall construction quality to create both two-part (Figure 1B) and three-part (Figure 1C) silicone master molds for subsequent injection casting of the inner core of the eye model. The mean and standard deviations of the master eye model dimensions used to create these master molds are shown in Table 1. The master molds were made with a two-part room temperature vulcanizing (RTV) silicone material (GI-1110, Silicones, Inc., High Point, NC) that was mixed according to label instructions. It was degassed in a 5-gallon vacuum chamber for 15 minutes (min) at -20 inches

(in.) of mercury (inHg) vacuum pressure prior to pouring in order to remove air bubbles introduced during mixing.

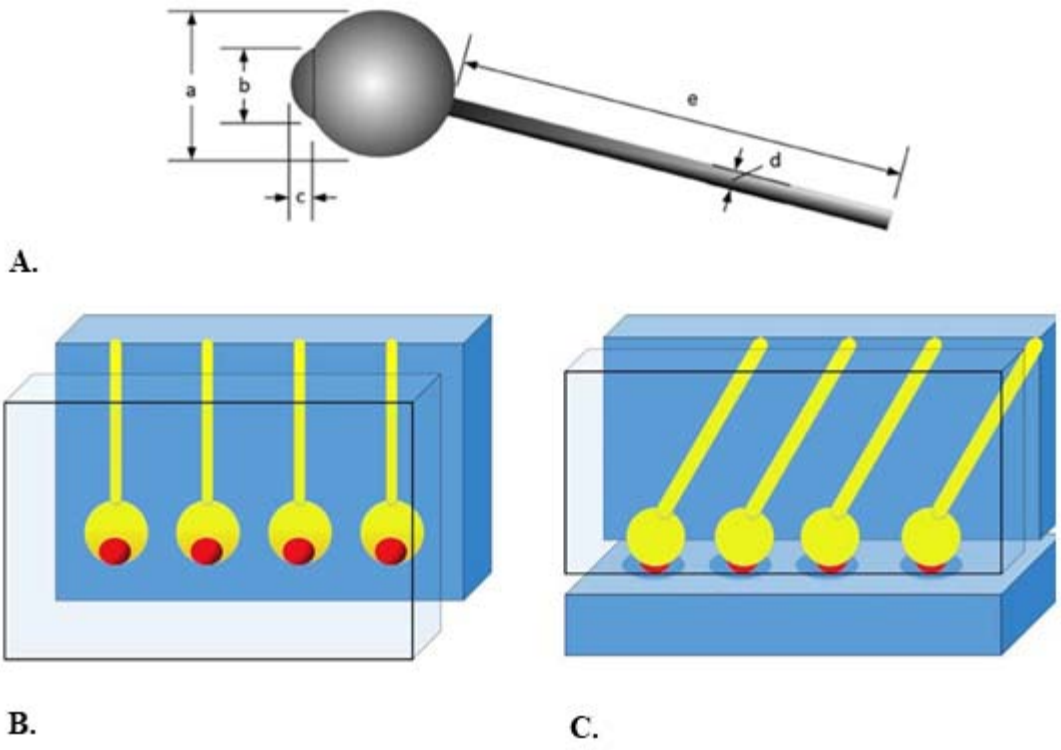

Figure 1. Constructing the Human Eye Model. A. Master model of eye. a) Posterior chamber diameter; b) Anterior chamber diameter; c) Anterior chamber height; d) Width of optic nerve; e) Length of optic nerve. B. Arrangement for using a two-part mold. C. Arrangement for using a three-part mold.

Table 1. Master Eye Model Statistics for the Casting of the Inner Core

Dimension	Mean (mm)	SD	N Value
Posterior Chamber Diameter @ Equator	24.80	0.42	6
Anterior Chamber Depth	3.47	0.17	6
Internal Anterior Chamber Diameter (Limbus to Limbus)	12.20	0.11	6
Optic Nerve Diameter	3.62	0.07	6

The two-part silicone molds were designed to make eye models of the corneoscleral shell and attached optic nerve without the option of having additional internal ocular anatomy modeled. The two-part mold uses a single injection of liquid gelatin to produce the inner core of the eye model. Each of the six wood master models was embedded into non-hardening oil-based tin clay that covered one-half of the globe and optic nerve in order to form the first half of the RTV silicone mold. After allowing this first half to cure overnight, the clay was removed, a release agent applied to the cured silicone, and the second half of the silicone mold was poured

and allowed to cure, thus completing the mold. The distal end of the wood dowel representing the optic nerve for each eye model formed the fill-port for casting the inner core.

The three-part molds were designed to allow experimentation in terms of adding internal components to the eye model, particularly a simulated iris and simulated crystalline lens with a supporting structure. The three-part mold design permits multiple injection events that build the internal components of the eye model in layers between the anterior and posterior chambers. The three-part molds required two sections of embedding clay, one for producing one-half of the posterior section of the globe and attached optic nerve, similar to the two-part mold-making process, and one for the complete anterior segment portion of the globe. The two posterior mold sections were poured individually in two separate steps in a manner similar to the two-part mold, followed by pouring of the anterior section of the mold as the third and final step of the master mold-making process.

Two-Part Mold Casting of the Inner Core

Casting the inner core was relatively straightforward. The silicone master molds were closed without the use of any release agent. Acrylic backing plates of 4-mm thickness were applied to the sides and base of the silicone master mold and held in place with multiple rubber bands in order to provide structural stability to the master mold during inner core casting. Gelatin solution was mixed in batches sufficient for producing six inner cores with a reserve in case of spillage or leakage. Specifically, 3 grams (g) of calcium chloride granules (C1016, Sigma-Aldrich, St. Louis, MO) were added to a 250-milliliter (-mL) beaker with 150 mL of distilled and deionized water at a pH acidity of 7.3 and a temperature of 70.0° Fahrenheit (F). Two drops of liquid food coloring (Neon!, McCormick, Inc., Hunt Valley, MD) were added to allow the inner core gelatin to be visible during the subsequent stages of the eye model casting process and during storage. The solution was stirred until the calcium chloride granules were completely dissolved. It was then equally divided between two beakers. One beaker was heated in a microwave oven until the solution was approximately 145°F. As the first half of the solution was heating, 8 g of porcine skin gelatin powder, Type A, with a 300-g bloom strength (G2500, Sigma-Aldrich, St. Louis, MO) was sprinkled across the remaining half of the room temperature liquid and slowly stirred to allow the gelatin to fully bloom (~90 seconds [s]). The heated solution was then added to the bloomed gelatin, and stirred slowly until the gelatin was incorporated fully into a liquid state. Slow stirring avoids incorporating air bubbles into the gelatin and the need to for degassing the solution. Additional experimentation included preparing inner cores with bovine skin gelatin powder, Type B, with a 225-g bloom strength (G9382, Sigma-Aldrich) using a similar protocol.

A 60-mL disposable syringe with a blunt-tip 16 gauge luer-lock needle and an attached 12-inch length of soft silicone tubing was used to inject the liquid gelatin solution into the silicone molds. Soft silicone tubing prevented damage to the inner walls of the silicone mold. The end of the tubing was inserted into the fill port, glided into the globe portion of the mold, and liquid gelatin was slowly injected while allowing air to escape from the top of the fill port. As gelatin emerged near the top of the fill-port, the injection continued as the tubing was removed in order to avoid trapping air within the optic nerve part of the mold. Each inner core requires a volume of slightly more than 15 mL of injected liquid gelatin, depending on the desired length of the optic nerve and any waste due to overflow. After all inner cores were filled,

the silicone mold was allowed to rest undisturbed at room temperature until the gelatin had initially set (~60 min). The silicone mold was then placed inside of a refrigerator and chilled thoroughly to a temperature of 34°F.

Three-Part Mold Casting of the Inner Core

Inner core casting with the three-part mold involved more steps than that of the two-part mold. First, the AC depression of the inner core in the third section of the mold was filled with gelatin and allowed to gel at room temperature. Because of the small volume involved, a 1-mL disposable syringe with a 21-gauge needle was used to fill the AC. Next, optional internal components (e.g., a simulated iris structure or a simulated crystalline lens) were positioned with surgical tweezers by placing them on top of the AC gelled component while aligning these with the geometric axis of the eye. Additional gelatin was then added to the anterior half of the inner core globe to fix the internal components in place after gelling at room temperature. Finally, the two remaining sections of the three-part mold were closed, and the final portion of the inner core representing the posterior chamber and optic nerve was injected through the fill port. Reheating of the gelatin reserve may be required when fabricating the inner cores with the three-part molds due to the additional time needed to assemble the internal components. Caution must be exercised during fabrication because injecting liquid gelatin that is too hot can cause the internal components to sink to the bottom of the mold or become misaligned.

Demolding the Inner Cores

Failure to chill completely the mold for several hours will cause the inner cores to fracture during demolding, often at the location of the optic nerve attachment. Therefore, chilling overnight was performed in addition to keeping the lower half of the mold on a tray of wet ice during demolding. After removal of the silicone mold from the refrigerator, the acrylic plates were removed. When opening the two-part silicone mold, the mold was placed on its side (thus becoming the lower section) with the anterior chamber section of the inner core facing up. When opening the three-part mold, the mold was completely inverted and the third section (i.e., the anterior part of the inner core) was removed first by breaking the seal along the edge of this section and lifting upward by starting at one end. The remaining sections were laid on one side, and the process for demolding was similar to that for the two-part mold described below.

The seal of the two-part mold was broken by running the tip of a flat spatula completely around the mold parting line. Starting with the globe side, the top half of the silicone mold was lifted starting at one corner and continuing across all of the inner cores. A soft-bristle brush was used to prevent the optic nerve from being lifted away from the globe if it tended to stick to the top half of the mold. All of the inner cores along with their simulated optic nerves must remain on the bottom half of the mold.

Typically, the gelatin near the distal end of the optic nerve at the filling port was exposed to air and dried during refrigeration, causing it to stick to both sides of the mold. The spatula was used to slice off this dried end of the optic nerve section without damaging the silicone mold, thus allowing the upper half of the mold to be completely released from the lower half and set aside. Again, using the spatula, the distal end of the simulated optic nerve was cut to the desired length (typically 50 mm). The nerve was released completely from the mold by pressing the

brush handle's blunt rounded tip (or a similar rounded tool with a diameter that fits into the silicone mold channel of the optic nerve), down and along the mold channel toward the globe, thereby gently lifting the gelatin out of the mold. Gently pressing the mold around the globe itself allowed the inner core to release from the silicone. Each inner core globe could then be removed by hand, taking care not to break off the attached optic nerve. Usually, the globe was grasped with the thumb and index finger and the optic nerve portion cradled by the remaining fingers. Laboratory gloves were worn during demolding to avoid the warmth of the fingertips from making fingerprint impressions on the inner core. Breakage of the optic nerve portion of the mold was usually attributed to rough handling, air trapped in the mold, inadequate chilling of the mold, or using an incorrect formulation of the gelatin that affected the bloom strength. Excess particles of gelatin were brushed off the inner core after demolding. After removal from the mold, the inner core was placed on its side at the bottom of a completely dry, low-profile, wide-diameter (~4 in.), flat-bottom container for casting of the corneoscleral shell.

Casting the Corneoscleral Shell

The corneoscleral shell of the surrogate human eye model was composed of an adjustable polymer hydrogel made from ionically crosslinked alginate, which has been shown through numerous studies to be a biocompatible material suitable for tissue engineering applications (Aljohani, Ullah, Zhang, & Yang, 2018; Becker, Preul, Bichard, Kipke, & McDougall, 2007; Bedian, Villalba-Rodriguez, Hernandez-Vargas, Parra-Saldivar, & Iqbal, 2017; Dvir-Ginzberg, Gamlieli-Bonshtein, Agbaria, & Cohen, 2003; Kirschning, Dibbert, & Drager, 2018; C. K. Kuo & Ma, 2001, 2008; S. M. Kuo, Wang, Weng, Lu, & Chang, 2005; Rowley, Madlambayan, & Mooney, 1999).

Alginate (alginic acid) is a byproduct of brown seaweed (Phacophycae). It is a hydrophilic, anionic linear polysaccharide chain composed of D-mannuronic acid and L-guluronic acid residues that are connected via 1,4-glycosidic linkage. Alginate organizes into 3D polymer hydrogel structures when exposed to calcium ions, thereby creating complex "egg-carton" crosslinks where adjacent guluronic acids are co-located and become ionically bound.

The alginate material for creating the hydrogel scaffold was derived from a solution composed of 20 g of sodium alginate powder (41900060-1, bioWORLD, Dublin, OH) mixed with 2000 mL of distilled water at a pH of 7.3 and a room temperature of 70.0°F for 5 minusing a blender set to a medium speed (e.g., speed setting #2 on an XL Blast blender, BL4000R, Black & Decker, Inc., Towson MD). The blended sodium alginate solution was poured into a beaker and degassed for ~30 min in a 5-gallon vacuum chamber at -20 inHg. The beaker was then removed from the vacuum chamber, covered tightly with cellophane, and stored overnight under refrigeration at 34°F. Prior to use, the liquid alginate solution was removed from refrigeration and allowed to return to room temperature (70.0°F). Unused alginate solution was stored under refrigeration for later use.

The flat-bottom container holding the inner core was placed on a laboratory orbital shaker (Orbi-Shaker XL, Benchmark Scientific, Edison, NJ), Shaking speed was set to 110 revolutions per minute (RPMs), and the automatic timer was set to the period of time needed to create a specific thickness of the hydrogel scaffold. The exact time was determined by experimentation that established a linear functional relationship between scaffold thickness and

immersion time as described in the Results. The calcium ions required for crosslinking the alginate into a 3D polymer scaffold came from the calcium chloride that was added to the inner core gelatin solution. The liquid sodium alginate solution was poured into the beaker away from the inner core, and the solution was allowed to rise from the bottom of the beaker to fully cover the inner core. Simultaneous with the pouring, the orbital shaker was started to prevent air from being trapped between the inner core and the hydrogel shell or within the hydrogel shell itself during crosslinking, as pouring the alginate solution directly over the inner core tended to trap air bubbles. The inner core was covered with alginate solution to a depth of approximately 15 mm while shaking. There was sufficient volume of the liquid alginate to allow the inner core to move freely both vertically and horizontally within the solution during shaking. It was critical that the distal end of the optic nerve remain free-floating and not contact the globe during this process to prevent fusion of the nerve sheath with the corneoscleral shell.

After the allotted time to create a shell of a desired thickness, the hydrogel-coated eye model was removed from the alginate solution and allowed to drain for approximately 60 s with the corneal surface facing up. This may be performed by cupping the eye model globe so that the optic nerve portion hangs down between two fingers of a gloved hand, or the globe can be placed on a cushioned rack that holds the eye model with the cornea facing up and the optic nerve hanging down to drain. The eye model was then placed in 400 mL of distilled water at 70.0°F, and shaken with the orbital shaker at 110 RPMs for at least 15 min to allow the hydrogel shell to continue to strengthen as the uncrosslinked excess alginate solution was rinsed away.

After rinsing, the eye model was stored under refrigeration at 34°F within screw-cap jars filled with fresh, sterile distilled water. Eye models were typically screened later the same day or on the following day for quality control in terms of shell thickness uniformity and shell shape consistency using non-contact optical methods, namely optical coherence tomography (Cirrus, Carl Zeiss-Meditec, Inc., Dublin, CA) and Scheimpflug imaging tomography (Pentacam HR, Oculus, Inc., Arlington, WA).

Hybridization of the Scaffold

The prototype of the eye model uses a basic alginate scaffold to define the shape and dimensions of the corneoscleral shell. Alginate scaffolds have viscoelastic properties that are desired for a hydrated interwoven polymer matrix, but they lack the resilience and mechanical strength imparted by collagen fibers comprising the extracellular matrix of living tissues (Kaklamani, Cheneler, Grover, Adams, & Bowen, 2014; Kuo & Ma, 2008; Sun & Tan, 2013). A variety of hybridized scaffolds incorporating alginate scaffolds with various synthetic or natural polymers are possible with this model, depending on the requirements of biocompatibility or strength. Hybridized hydrogel scaffolds have been described extensively in bioengineering literature (Eslami et al., 2014; Mekhileri et al., 2018; Moller et al., 2011; Shim, Kim, Park, Park, & Cho, 2011; Tsang & Bhatia, 2004; Weinstein-Oppenheimer et al., 2017; Xu, Jha, Harrington, Farach-Carson, & Jia, 2012). In particular, synthetic matrixes that incorporate polyvinyl alcohol (PVA) with sodium alginate in proportions desired for achieving specific strengths are being studied. Polyvinyl alcohol (PVA) can be crosslinked with freeze-thaw methods or ultraviolet (UV) light once the alginate scaffold forms by ionic cross-linking with calcium. Other variants of hybrid hydrogels are open to experimentation with this eye model, including the inclusion of collagen, methyl acrylate, or glutaraldehyde as UV-cross-linkable materials (Izadifar, Chapman,

Babyn, Chen, & Kelly, 2018; Moller et al., 2011). Separating the process of defining the eye model's shape using ionically crosslinked sodium alginate from the process of strengthening the model with PVA or another material that depends on photo-activated or mechanical crosslinking appears to be optimal for maintaining optimum control over the quality of the final product. Cross-linking the eye model for strength early in the construction process may "lock-in" an undesired form or surface texture. Additional variations of the strengthening process include over-coating the alginate scaffold, or alternating between thin layers of the alginate scaffold with other interpenetrating scaffold types (Catros et al., 2012; Kundu, Shim, Jang, Kim, & Cho, 2015). Future reports on the eye model will include descriptions of variants utilizing hybridized hydrogels.

Pressurization of the Eye Model

The eye model in storage relies on the inner core to maintain structural support of the shell. When tested by tonometry in this configuration (Tono-Pen XL, Reichert, Inc., Depew, NY), the model gave an ostensible IOP of approximately 15 mmHg, which closely resembles the normal physiological IOP of the living human eye. While the basic gelatin-filled eye model may be adequate for a specific purpose, in most applications a completely liquid or semi-gelatinous internal configuration is needed such that the IOP can be precisely adjusted via a manometer system (i.e., cannulation of the eye).

Preparing the model for cannulation begins with the creation of the main port. Care should be taken to not allow the surface of the eye model to dry out during the port connection process by wrapping the exposed eye model in wet gauze and rewetting as needed. The exposed distal tip of the simulated optic nerve sheath was excised with straight surgical scissors, thereby reserving a length of the sheath that remains attached to the globe, and which was sufficiently long enough to pass entirely into the cranium when the globe of the eye model was placed within the orbital eye mount at an anatomically correct position. A short length of the inner core gelatin (~5 mm) was then squeezed out of the end of the sheath with the fingertips and removed. The barbed end of a ⅛-inch luer-lock connector attached to tubing from the manometer system was then inserted into the open lumen of the optic nerve sheath (Figure 2A). This port connector was customized such that it and the connected tubing could pass freely through the optic canal of the orbit coming from the cranium section of the headform. Fluid from the manometer system was flowing under a low positive pressure such that no air was introduced into the lumen while the barbed connector was inserted. If air bubbles consistently occur when connecting the port, immerse the eye model and the end of the barbed connector in a bath of the manometer system fluid such that no air is trapped when the barbed end is inserted. Additionally, it is possible to allow air to escape the manometry line but allowing the air bubble to float up to the top of the fluid reservoir where it can be removed easily.

After insertion of the port, the sheath was tied off to maintain a reliable, leak-free connection to the manometer system. Using a 15-in. length of flat, waxed dental floss, the outside of the sheath was wrapped three times immediately behind the barb, with the ribbon floss laid flat against the sheath surface. The slack was then taken up, and the free ends tied with double square knots and the ends trimmed close to the knot. The pressure in the manometer was raised slightly to confirm that the port connection did not leak. If leaking, the knot was cut off and the process repeated. Maintaining a longer sheath length allows the user to completely cut

off the distal end of the sheath and start over in case the hydrogel has been cheese-wired by the floss.

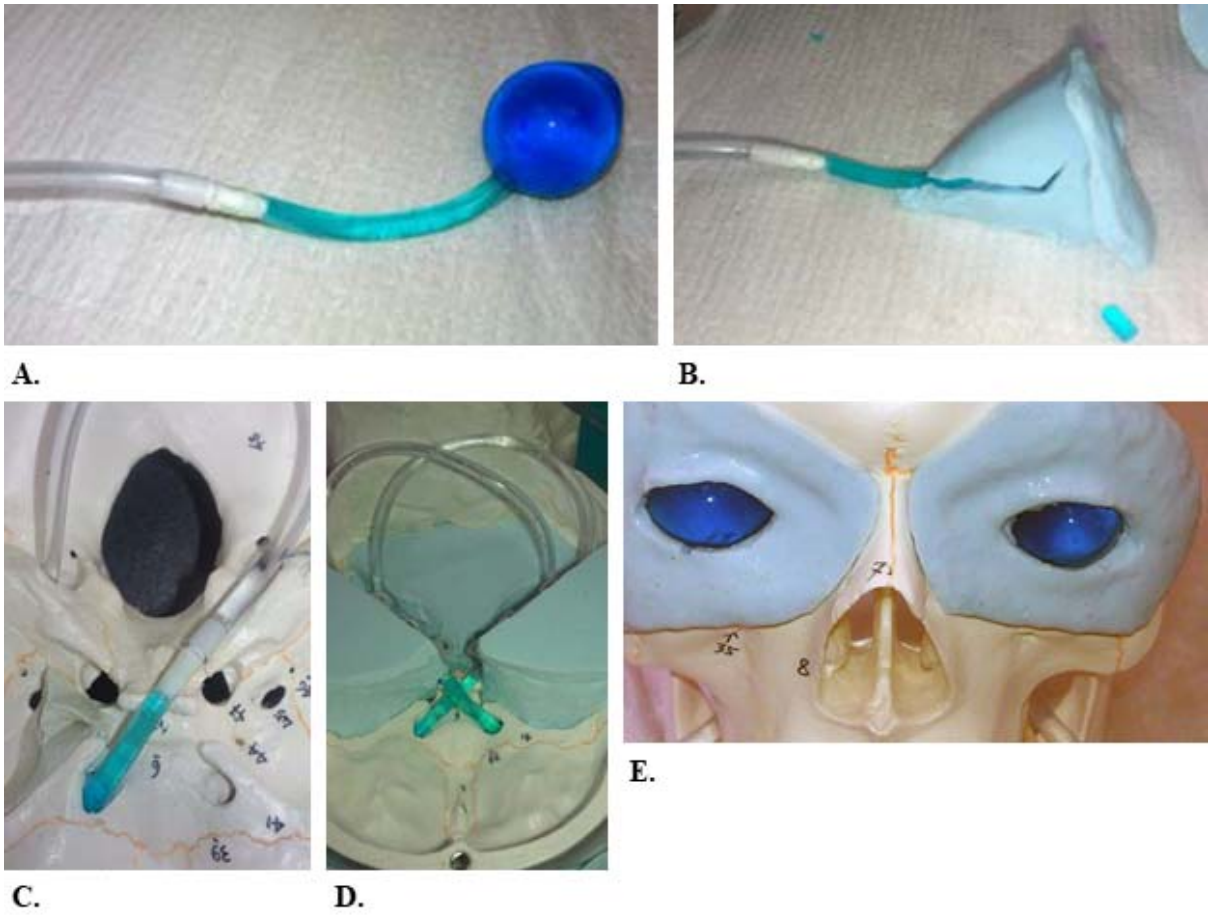

Figure 2. Connecting the Human Eye Model. A. Eye model ported to cannula line. B. Eye model inserted into eye holder. C. View of port connection from inside the cranium. D. View of overlapping ported ends of the optics nerves for mounting two eye models. E. Dual eye mounting into the skull headform.

The entire eye model was then immersed in warm water (~130°F) for several minutes or until the gelatin inner core was liquefied. The contents of the eye model were then replaced either by a cyclical process of suction and backfilling through the manometer line until the gelatin was dilutes and completely removed as indicated by the lack of dye color, or more quickly evacuated by the use of a co-linear input tube introduced via the leak-free catheter attachment to the manometer. This co-linear tube was a narrow gauge internal fill tube (~1 mm in diameter) located within the larger manometer tubing and extending to the end of the barbed portion of the main port. The fill fluid was then injected through the inner tube and evacuated simultaneously via the external tube. The use of a customized, sealed multi-port catheter arrangement of the manometer system allowed not only the precise placement of the internal fill tube, but also the introduction of internal instruments into the eye model, such as individual fiber-optic cables.

Mounting the Eye Model

It should be noted that in typical use, the primary manometer tubing must pass through the optic canal opening of the bony orbit before porting the eye model. The current prototype of the eye holder made from silicone materials allowed the eye model to be loaded entirely from the back so it did not interfere with the porting of the eye model (Figure 2B). A potential space exists within the eye holder to allow limited movement of the globe and simulated nerve within the space. The potential space behind the globe was filled with petroleum jelly to simulate the density of orbital fat. Failure to fill this space would leave a pocket of air behind the eye, which would interfere with the propagation of a shock wave and provide unreliable results with the model. Before mounting the eye, the preferred angular orientation of the optic nerve as it exits the globe was determined, and the globe rotated about its geometric axis in order to orient the nerve toward the optic canal prior to tying off the port adapter. Orienting the nerve in this manner was helpful because the inherent stiffness of the manometer tubing tended to limit the ability to correct for a misalignment once the eye model was mounted into the orbit of the headform.

Prior to placing the eye holder into the orbit, it was helpful to rotate the headform so that the orbital openings were facing upwards, which allowed gravity to help position the eye holder fully into the orbit as the manometer tubing was retracted into the cranium portion of the headform. When mounted correctly, the end of the simulated optic nerve should pass easily into the optic canal, and the main port connection should be clearly visible near the optic chiasm inside the cranium indicating the optic nerve is fully extended within the orbit (Figure 2C). A means of supporting and stabilizing the manometer tubing inside the cranium of the headform was deemed necessary to prevent the weight of the manometer line from tearing out the port or pinching the optic nerve sheath closed, which would restrict pressurization of the globe.

If the opposite orbit of the headform was also being used, the second eye model was mounted using the same process described above. When the eye holder for the second eye was positioned, the two fluid-filled sheaths overlapped one another in the area of the optic chiasm. Therefore, it was found helpful to have one of the optic nerve sheaths left longer such that the barbed ports did not directly overlie one another in the area of the chiasm, but rather the two ports were offset slightly (Figure 2D). After mounting, the ends of the exposed sheaths were covered with moist gauze to prevent drying.

The final checklist included the following: checking for manometry leaks, checking that the cornea of the eye model is oriented in the intended direction (Figure 2E), applying a thin layer of mineral oil to the anterior segment of the model to prevent drying, checking the level of IOP applied to the eye model, checking that flow in the manometry lines was not restricted, and checking the final position of any internal instrumentation. Internal instrumentation position was verified either by gauging the cable length passing into the catheter, or by visually confirming the location of the tip of the cable by looking into the globe as it was back-illuminated. However, direct visualization of internal instruments may not be possible depending on whether there is a loss of transparency when scaffold hybridization is used. Therefore, the use of an external imaging system that can locate objects inside the orbit, such as an ultrasound device, may be helpful.

Eye Model Storage

Typically, the eye model was used the following day after production. When prepared carefully under sterile laboratory conditions, the eye model has been amenable to storage for at least two weeks under refrigeration in sealed jars. Typically, any dye used to visualize the inner core will diffuse out during storage and into the surrounding storage media. Long-term storage methods remain under consideration, but would likely include the use antifungal preservatives and preparation of the model under strict clean-room laboratory conditions. Ultraviolet (UV) radiation used to crosslink a hybridized form of the scaffold, has an added benefit of being germicidal. Methods of preservation similar to those used for storing commercial hydrogel contact lenses would be acceptable.

Results

Scaffold Design

The novelty of the prototype eye model scaffold construction process is that a completely enclosed corneoscleral shell is produced in a single event when a precisely shaped inner core composed of solidified porcine gelatin infused with calcium chloride is immersed into a sodium alginate solution. The presence of calcium ions expressed from the gelatin initiates the crosslinking of the alginate, thereby creating the hydrogel shell (Figure 3A). The hydrogel shell effectively disappears in water due to the index of refraction of the shell being essentially identical to the water in which it is immersed. To aid in production and use of the eye model, the inner core was dyed with food coloring to allow it to be more easily seen. The thickness of the ionically-crosslinked hydrogel shell is determined largely by the deposition rate of the alginate. Therefore, controlling the time of exposure of the inner core to the liquid alginate solution determines the desired thickness of the corneoscleral shell, which can be confirmed subsequently by optical coherence tomography (OCT) measurements (Figure 3B) or by Scheimpflug-based tomography (Figure 3C).

This space is intentionally blank.

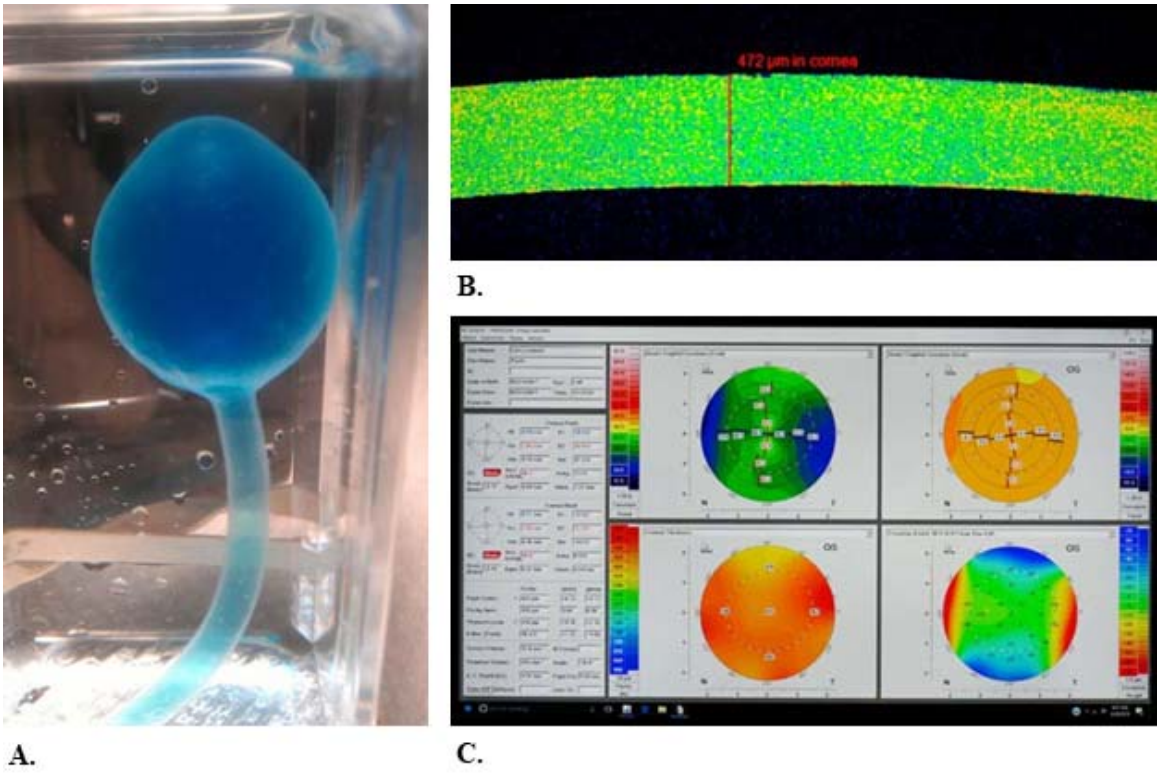

Figure 3. Visualizing the Human Eye Model. A. Completed scaffold. B. Zeiss optical coherence tomography (OCT) view of hydrogel shell in cross-section. C. Pentacam HR display of the cornea portion of the model.

Alginate Concentration

Experimental testing was performed to determine an acceptable concentration level of the sodium alginate immersion solution for a fixed calcium chloride concentration of the inner core in order to produce the eye model. Through trial and error, a 1% solution of 20g of sodium alginate to 2,000 mL of distilled water was determined to produce controllable shells of consistent scaffold thickness with smooth, optical-quality surfaces. Immersion solutions with more highly concentrated sodium alginate solutions (>3%) produced shells that tended to have irregular thickness and of overall lower quality due to roughly textured outer surfaces. Conversely, shells made with lower concentrations of alginate (~0.5%) formed scaffolds that tended to be consistently thin and fragile such that the scaffold easily broke apart with normal handing, and had low bursting strengths when the eye model was pressurized.

Other factors that affected shell quality included the speed of the orbital shaker and the volume of the alginate immersion bath. If the inner core was not immersed to a sufficient depth and lacked sufficient movement of the alginate solution, the thickness of the shell lacked uniformity, typically with one side of the globe being appreciably thinner than the rest. The alginate bath temperature was fixed by the room temperature at 70.0°F, which produced consistent results; however, during a brief period when the air conditioning in the laboratory varied by several degrees, the shell thickness became less predictable. Ideally, a temperature-regulated water bath should be used in maintaining the temperature of the solutions.

Calcium Concentration

Standardizing on a 1% liquid alginate immersion solution, refinement of the alginate deposition rate over time was determined for 3 different calcium ion concentrations of the inner core (Figure 4A). Through experimentation, a 2% solution composed of 3 g of calcium chloride to 150 mL of distilled water produced alginate scaffolds with good shell quality and a predictable thickness that could be controlled by the length of exposure time to the liquid alginate solution. Both optical coherence tomography (OCT) and Scheimpflug imaging tomography methods were used to verify the shell thickness.

Experiments with a Type B bovine gelatin for inner core production were found to be unsuccessful. Inner cores made with Type B gelatin remained soft and fractured easily during the demolding stage. Altering the gelatin concentration was not helpful toward increasing the strength of the inner cores. In particular, the failure rate for the Type B gelatin approached 100% with the most common failure being fractures of the simulated optic nerve. In comparison, the Type A porcine gelatin had a nerve retention rate of 100% with an experienced user.

While other factors such as pH, temperature, and the stirring rate during alginate immersion must be controlled, the concentration of calcium was a critical determinant of a predictable shell thickness and repeatability. Inner cores made with a higher concentration of calcium (>3%) produced thicker shells more rapidly, but the accuracy of producing a specific shell thickness was degraded because of the inability to immediately stop the crosslinking process after a specific elapsed time in the alginate solution. While, the use of low calcium concentrations of around 0.5% produced hydrogel shells with good thickness predictability, they required significantly longer immersion times in the alginate to achieve the desired thickness. Longer times in the alginate tended to produce more quality control errors, such as a greater likelihood that the distal end of the optic nerve sheath would attach itself to the globe.

Thickness Accuracy and Repeatability

Using all six of the eye mold positions, four separate attempts (N = 24) were made to create eye models with a 1,000-μm central corneal thickness (CCT) at the corneal apex. The mean (±SD) CCT result measured by a single operator with a Pentacam HR tomography system was 948.84 ± 29.55 μm. In normal living human corneas, the reported variance of CCT measured by the Pentacam HR has been on the order of ±30.71 μm in the human. Since each of the mold positions was formed from a unique master mold intended to create corneal curvatures between 38 and 44 diopters, the resulting CCT accuracy is acceptable for early development of the prototype. The SD value suggests that variance is acceptably low, and the method is repeatable and in agreement with biological variability in living human eyes.

Curvature and Shell Thickness Effects and Artifacts

Producing shells of relatively greater thickness should theoretically affect the overall curvature of the surface. Curvature is inversely proportional to its radius of curvature, so increasing the shell thickness effectively increases the radius of curvature, resulting in the surface becoming relatively flatter. There is a statistically significant ($p < 0.001$) and moderately strong ($R^2 = 0.781$) linear relationship between the mean keratometry curvature of the modeled

corneal surface and the time of exposure to alginate, confirming that this effect does take place (Figure 4B). This should be taken into account when designing eye models of a specific thickness and curvature.

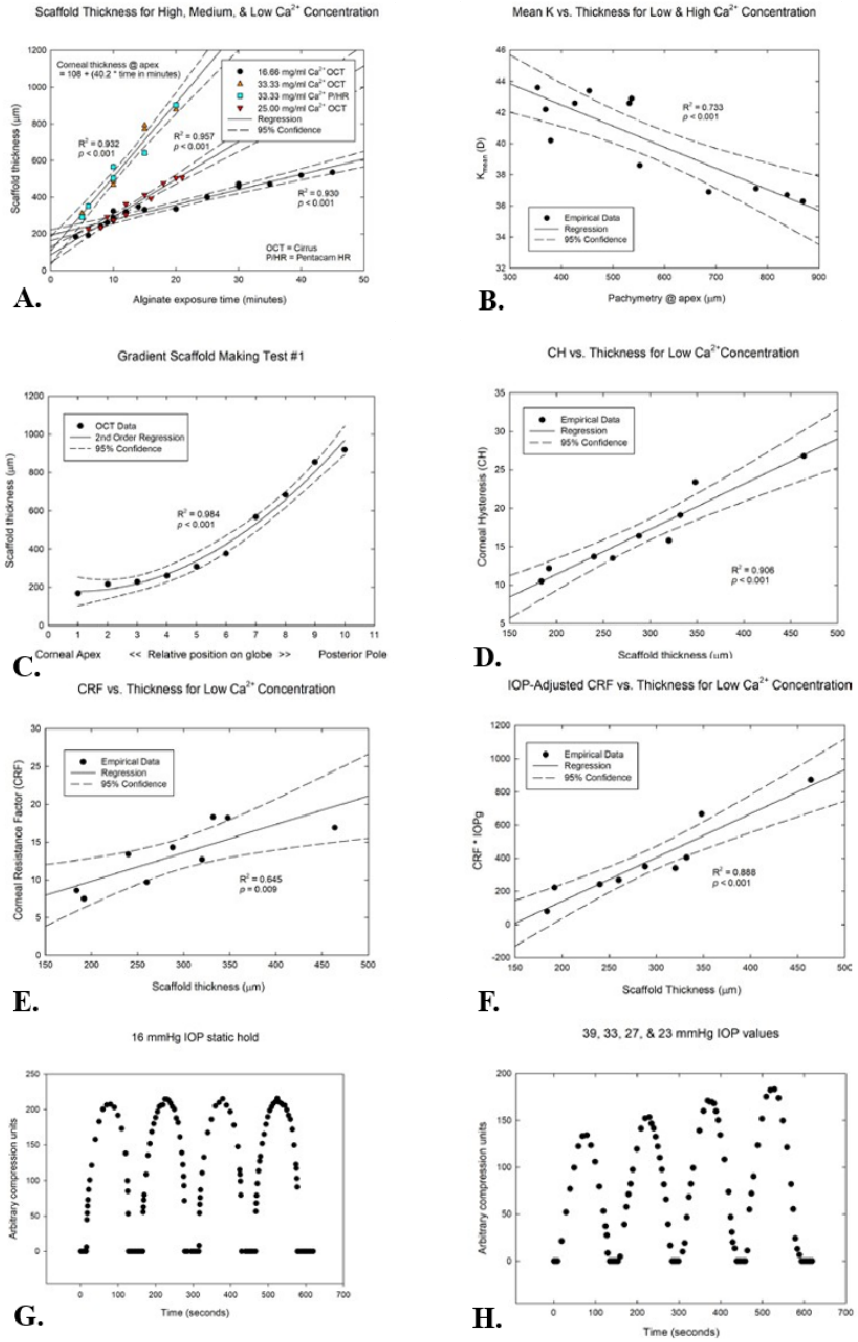

Figure 4. Manipulating the Human Eye Model. A. Calcium concentration controls shell thickness. B. Change in corneal curvature with alginate exposure. C. Control of corneal thickness by distance from the apex. D.: Corneal Hysteresis (CH) testing. E.: Corneal Resistance Factor (CRF) testing. F. CRF with IOP weighting. G. Constant IOP load testing with cyclical compression of the eye globe. H. Ramped IOP Load with cyclical compression of the eye globe.

Producing Variable Thickness

Additional experimentation into differentially controlling the exposure time to liquid alginate from the apex to the peripheral cornea by vertically mounting the inner core during immersion was shown to produce corneas with a thicker periphery and a relatively thinner apex (Figure 4C). This creates a more accurate representation of true corneal thickness. This approach requires precise control of the liquid alginate delivery rate, making it more suitable for automated production methods. The application of the eye model will likely dictate whether such precise specifications are needed.

Biomechanics

Results of the biomechanical characteristics of the completed eye model scaffolds was recorded using a clinical instrument that evaluated corneal hysteresis (CH) and corneal resistance factor (CRF) (Franco & Lira, 2009; Ortiz, Pinero, Shabayek, Arnalich-Montiel, & Alio, 2007; Shah, Laiquzzaman, Bhojwani, Mantry, & Cunliffe, 2007). While this clinical device is designed and calibrated for use with living eyes, the results of such testing can be informative, particularly in that testing would illustrate that the eye model at this stage lacks structural resilience and stiffening such as that created by the presence of interwoven collagen fibers in the living eye. The IOP of the eye models were adjusted through cannulation to a nominal pressure of 15 to 18 mm Hg. Only distilled water was used as the intraocular medium. Shell thicknesses between 150 and 500 μm were tested simultaneously for CH and CRF using the Reichert ORA device. Figure 4D illustrates the linear relation of CH as a function of thickness. The relationship was strong and statistically significant ($R^2 = 0.906$; $p < 0.001$). CH was more than twice the value reported in living human eyes for a normal corneal thickness (~29 vs. 10.8), although the overall trend with thickness change was similar. This result was unexpected because the alginate scaffold alone was expected to be more pliable, which was thought to allow it to return to its original shape faster (i.e., show a more limited change in IOP between the stages of loading and unloading applanation by the air puff). Further investigations are needed to understand this result.

Figure 4E shows the linear relationship of the corneal resistance factor CRF for shell thickness from 150 to 500 μm. The CRF values were moderately strong and statistically significant ($R^2 = 0.645$; $p = 0.009$). When weighted by IOP, the CRF values showed a stronger correlation that was also significant (Figure 4F; $R^2 = 0.888$; $p < 0.001$). These data suggest that for a shell thickness equivalent to a normal human cornea, the CRF is approximately twice the amount found in the living human eye (~20 vs. 11.0), which is a result similar to that seen with CH.

Additional preliminary work has been carried out in performing whole globe compression tests of the intact, pressurized eye models. In this study, back-illuminated globes of 1 mm shell thickness were compressed between glass plates using a microprocessor-controlled loading system. Loading and unloading for 4 cycles with a constant 16 mm Hg IOP is shown in Figure 4G, and suggests that the shells are not prone to leakage or strain damage under the given load conditions. The initial cycle appears to be indicative of slightly reduced strain compared to the following 3 cycles, which can be interpreted as an initial conditioning cycle. Similarly, load and unloading was performed with step-wise changes in IOP (39, 33, 27, and 23 mmHg) induced

between cycles (Figure 4H). Results were consistent with performance expectations.

Discussion

The human eye is a fluid-filled, globe-shaped structure with a thin-walled, stress-bearing external shell composed of interwoven collagen fiber layers surrounding the internal cellular structures and neurosensory pathways responsible for vision. The vitreous humor within the posterior chamber of the eye is a hydrated gelatinous structure, while the watery aqueous humor of the anterior chamber is responsible for intraocular pressure. This pressure imparts tensile stress to the corneoscleral shell, thereby enabling the eye to be structurally and optically stable. Although the collagen of the corneoscleral shell is inherently resistant to structural damage, the structurally weaker tissues within the eye lack this resilience. Moreover, the effects of overpressure upon the delicate tissues within the fluid-filled eye are not well characterized in humans. The back and sides of the eye are ordinarily protected by the surrounding funnel-shaped, bony orbit; however, this same structure has been implicated in reflecting, concentrating, and potentially amplifying the effects of a shock wave entering the orbit. In particular, the optic canal at the back of the orbit where the optic nerve passes into the cranium is presumed to be a focal point for overpressure entering the cranium and affecting the midbrain.

The USAARL-Smolek eye model is a bioengineered, dimensionally accurate, pressurized, fluid-filled representation of the corneoscleral shell and optic nerve sheath of the human eye composed of a modifiable, ionically-crosslinked hydrogel scaffold. The model is intended to be a first-order approximation of the anatomy and biomechanical properties of the living eye. It can be instrumented with miniature data collection sensors to measure overpressure within the eye with minimal influence upon the propagation of the shock wave. The inclusion of a simulated optic nerve allows overpressure and trauma to be evaluated anywhere along the length of the nerve. A bioengineered eye model eliminates many uncontrolled aspects of biological variance typically found when using post-mortem human or animal eyes, as well as making it possible to conduct experiments with large sample sizes to reduce further statistical variance.

The alginate-based scaffold can be hybridized for augmented biomechanical strength by the inclusion of natural or synthetic polymers or natural collagen fibers. Final strength can be controlled by a freeze-thaw or UV-crosslinking process such that the scaffold form and strength are controlled by independent crosslinking mechanisms. This approach allows the desired form to be established prior to locking-in the material strength. Bio-compatible versions of the scaffold can be embedded with living cells in order to evaluate the biological consequences of ocular trauma over time. The USAARL-Smolek model is more suitable than flat scaffolds for understanding the effect of complex patterns of overpressure on cell death or cellular expression. Immunohistochemical assays as well as traditional histology sectioning methods can then be used to assess outcomes for the eye model relative to blast parameters of the test. Perfusion under normal IOP levels is accomplished via cannulation of the simulated optic nerve.

As with any prototype, there are limitations to be addressed as an improved version is developed. The thickness of the corneal component tends to be uniform and identical to the thickness of the scleral component. Ideally, the central cornea should be thinner and the periphery of the cornea relatively thicker. As we demonstrated in the Results, the exposure time

for the corneal alginate immersion can be controlled in a gradient manner such that the corneal apex can be made relatively thinner than the periphery. Additionally, the thickness of the sclera is not uniform in the living eye, but tends to be thinner around the equator and posterior to where extraocular muscle tendon attachments are located. Since the eye model is intended to be an approximation to the living eye and the analysis of the shell properties are meant to be simplified, a high level of accuracy and precision in terms of thickness may be unnecessary. Use of the eye model in future studies will guide further development.

Conclusions

In conclusion, the human surrogate eye model is a new approach to understanding how shock waves induce ocular PBI. It is also designed to serve as a test article for evaluating the blast protection ability of protective eyewear. This model has other potential applications including serving as a perfusable scaffold for growing artificial corneal tissue for grafting, as well as performing as a medical simulation for surgical training.

References

Aljohani, W., Ullah, M. W., Zhang, X., & Yang, G. (2018). Bioprinting and its applications in tissue engineering and regenerative medicine. *International Journal of Biological Macromolecules, 107*(Pt A), 261-275. doi:10.1016/j.ijbiomac.2017.08.171

Atchison, D. A., Jones, C. E., Schmid, K. L., Pritchard, N., Pope, J. M., Strugnell, W. E., & Riley, R. A. (2004). Eye shape in emmetropia and myopia. *Investigative Ophthalmology and Visual Science, 45*(10), 3380-3386. doi:10.1167/iovs.04-0292

Beamer, M., Tummala, S. R., Gullotti, D., Kopil, C., Gorka, S., Ted, A., . . . Meaney, D. F. (2016). Primary blast injury causes cognitive impairments and hippocampal circuit alterations. *Experimental Neurology, 283*(Pt A), 16-28. doi:10.1016/j.expneurol.2016.05.025

Becker, T. A., Preul, M. C., Bichard, W. D., Kipke, D. R., & McDougall, C. G. (2007). Preliminary investigation of calcium alginate gel as a biocompatible material for endovascular aneurysm embolization in vivo. *Neurosurgery, 60*(6), 1119-1127; discussion 1127-1118. doi:10.1227/01.NEU.0000255447.90106.12

Bedian, L., Villalba-Rodriguez, A. M., Hernandez-Vargas, G., Parra-Saldivar, R., & Iqbal, H. M. (2017). Bio-based materials with novel characteristics for tissue engineering applications - A review. *International Journal of Biological Macromolecules, 98*, 837-846. doi:10.1016/j.ijbiomac.2017.02.048

Beiran, I., & Miller, B. (1992). Pure ocular blast injury. *American Journal of Ophthalmology, 114*(4), 504-505. doi:10.1016/s0002-9394(14)71868-9

Bhardwaj, R., Ziegler, K., Seo, J. H., Ramesh, K. T., & Nguyen, T. D. (2014). A computational model of blast loading on the human eye. *Biomechanics and Modeling in Mechanobiology, 13*(1), 123-140. doi:10.1007/s10237-013-0490-3

Catros, S., Guillemot, F., Nandakumar, A., Ziane, S., Moroni, L., Habibovic, P., . . . Fricain, J. C. (2012). Layer-by-layer tissue microfabrication supports cell proliferation in vitro and in vivo. *Tissue Engineering Part C Methods, 18*(1), 62-70. doi:10.1089/ten.TEC.2011.0382

Chalioulias, K., Sim, K. T., & Scott, R. (2007). Retinal sequelae of primary ocular blast injuries. *Journal of the Royal Army Medical Corps, 153*(2), 124-125. doi:10.1136/jramc-153-02-11

Crowley, J. S., Brozoski, F. T., Duma, S. M., & Kennedy, E. A. (2009). Development of the Facial and Ocular Countermeasures Safety (FOCUS) headform. *Aviation Space and Environmental Medicine, 80*(9), 831.

Duma, S. M., Kress, T. A., Porta, D. J., Martin, P. G., Simmons, R. J., & Alexander, C. L. (1997). An experimental study of airbag impact to the orbit using an instrumented Hybrid III headform. *Biomedical Sciences Instrumentation, 33*, 59-64.

Dvir-Ginzberg, M., Gamlieli-Bonshtein, I., Agbaria, R., & Cohen, S. (2003). Liver tissue engineering within alginate scaffolds: effects of cell-seeding density on hepatocyte viability, morphology, and function. *Tissue Engineering, 9*(4), 757-766. doi:10.1089/107632703768247430

Erb-Eigner, K., Hirnschall, N., Hackl, C., Schmidt, C., Asbach, P., & Findl, O. (2015). Predicting Lens Diameter: Ocular Biometry With High-Resolution MRI. *Investigative Ophthalmology and Visual Science, 56*(11), 6847-6854. doi:10.1167/iovs.15-17228

Eslami, M., Vrana, N. E., Zorlutuna, P., Sant, S., Jung, S., Masoumi, N., . . . Khademhosseini, A. (2014). Fiber-reinforced hydrogel scaffolds for heart valve tissue engineering. *Journal of Biomaterials Applications, 29*(3), 399-410. doi:10.1177/0885328214530589

Fontana, S. T., & Brubaker, R. F. (1980). Volume and depth of the anterior chamber in the normal aging human eye. *Archives of Ophthalmology, 98*(10), 1803-1808. doi:10.1001/archopht.1980.01020040655013

Franco, S., & Lira, M. (2009). Biomechanical properties of the cornea measured by the Ocular Response Analyzer and their association with intraocular pressure and the central corneal curvature. *Clinical & Experimental Optometry, 92*(6), 469-475. doi:10.1111/j.1444-0938.2009.00414.x

Garner, J., & Brett, S. J. (2007). Mechanisms of injury by explosive devices. *Anesthesiology Clinics, 25*(1), 147-160, x. doi:10.1016/j.anclin.2006.11.002

Gilmartin, B., Nagra, M., & Logan, N. S. (2013). Shape of the posterior vitreous chamber in human emmetropia and myopia. *Investigative Ophthalmology and Visual Science, 54*(12), 7240-7251. doi:10.1167/iovs.13-12920

Hubbard, W. B., Hall, C., Siva Sai Suijith Sajja, V., Lavik, E., & VandeVord, P. (2014). Examining lethality risk for rodent studies of primary blast lung injury. *Biomedical Sciences Instrumentation, 50*, 92-99.

Izadifar, M., Chapman, D., Babyn, P., Chen, X., & Kelly, M. E. (2018). UV-Assisted 3D Bioprinting of Nanoreinforced Hybrid Cardiac Patch for Myocardial Tissue Engineering. *Tissue Engineering Part C Methods, 24*(2), 74-88. doi:10.1089/ten.TEC.2017.0346

Kaklamani, G., Cheneler, D., Grover, L. M., Adams, M. J., & Bowen, J. (2014). Mechanical properties of alginate hydrogels manufactured using external gelation. *Journal of the Mechanical Behavior of Biomedical Materials, 36*, 135-142. doi:10.1016/j.jmbbm.2014.04.013

Kennedy, E. A., Inzana, J. A., McNally, C., Duma, S. M., Depinet, P. J., Sullenberger, K. H., . . . Brozoski, F. T. (2007). Development and validation of a synthetic eye and orbit for estimating the potential for globe rupture due to specific impact conditions. *Stapp Car Crash Journal, 51*, 381-400.

Kirschning, A., Dibbert, N., & Drager, G. (2018). Chemical Functionalization of

Polysaccharides-Towards Biocompatible Hydrogels for Biomedical Applications. *Chemistry, 24*(6), 1231-1240. doi:10.1002/chem.201701906

Kundu, J., Shim, J. H., Jang, J., Kim, S. W., & Cho, D. W. (2015). An additive manufacturing-based PCL-alginate-chondrocyte bioprinted scaffold for cartilage tissue engineering. *Journal of Tissue Engineering and Regenerative Medicine, 9*(11), 1286-1297. doi:10.1002/term.1682

Kuo, C. K., & Ma, P. X. (2001). Ionically crosslinked alginate hydrogels as scaffolds for tissue engineering: part 1. Structure, gelation rate and mechanical properties. *Biomaterials, 22*(6), 511-521. doi:10.1016/s0142-9612(00)00201-5

Kuo, C. K., & Ma, P. X. (2008). Maintaining dimensions and mechanical properties of ionically crosslinked alginate hydrogel scaffolds in vitro. *Journal of Biomedical Materials Research: Part A, 84*(4), 899-907. doi:10.1002/jbm.a.31375

Kuo, S. M., Wang, Y. J., Weng, C. L., Lu, H. E., & Chang, S. J. (2005). Influence of alginate on type II collagen fibrillogenesis. *Journal of Materials Science: Materials in Medicine, 16*(6), 525-531. doi:10.1007/s10856-005-0528-x

Lo, M., Capo-Aponte, J. E., Wise, D., Simpson, D., Barrett, A., Giffin, R., . . . Temme, L. A. (2013). *Ocular Battle Injuries among US Military Personnel, 2002-2011*. Retrieved from

Mekhileri, N. V., Lim, K. S., Brown, G. C. J., Mutreja, I., Schon, B. S., Hooper, G. J., & Woodfield, T. B. F. (2018). Automated 3D bioassembly of micro-tissues for biofabrication of hybrid tissue engineered constructs. *Biofabrication, 10*(2), 024103. doi:10.1088/1758-5090/aa9ef1

Moller, L., Krause, A., Dahlmann, J., Gruh, I., Kirschning, A., & Drager, G. (2011). Preparation and evaluation of hydrogel-composites from methacrylated hyaluronic acid, alginate, and gelatin for tissue engineering. *International Journal of Artificial Organs, 34*(2), 93-102.

Norman, R. E., Flanagan, J. G., Rausch, S. M., Sigal, I. A., Tertinegg, I., Eilaghi, A., . . . Ethier, C. R. (2010). Dimensions of the human sclera: Thickness measurement and regional changes with axial length. *Experimental Eye Research, 90*(2), 277-284. doi:10.1016/j.exer.2009.11.001

Ortiz, D., Pinero, D., Shabayek, M. H., Arnalich-Montiel, F., & Alio, J. L. (2007). Corneal biomechanical properties in normal, post-laser in situ keratomileusis, and keratoconic eyes. *Journal of Cataract and Refractive Surgery, 33*(8), 1371-1375. doi:10.1016/j.jcrs.2007.04.021

Petras, J. M., Bauman, R. A., & Elsayed, N. M. (1997). Visual system degeneration induced by blast overpressure. *Toxicology, 121*(1), 41-49. doi:10.1016/s0300-483x(97)03654-8

Rigas, F., & Sklavounos, S. (2005). Experimentally validated 3-D simulation of shock waves generated by dense explosives in confined complex geometries. *Journal of Hazardous Materials, 121*(1-3), 23-30. doi:10.1016/j.jhazmat.2005.01.031

Rowley, J. A., Madlambayan, G., & Mooney, D. J. (1999). Alginate hydrogels as synthetic extracellular matrix materials. *Biomaterials, 20*(1), 45-53. doi:10.1016/s0142-9612(98)00107-0

Scott, T. E., Kirkman, E., Haque, M., Gibb, I. E., Mahoney, P., & Hardman, J. G. (2017). Primary blast lung injury - a review. *British Journal of Anaesthesia, 118*(3), 311-316. doi:10.1093/bja/aew385

Shah, S., Laiquzzaman, M., Bhojwani, R., Mantry, S., & Cunliffe, I. (2007). Assessment of the biomechanical properties of the cornea with the ocular response analyzer in normal and keratoconic eyes. *Investigative Ophthalmology and Visual Science, 48*(7), 3026-3031. doi:10.1167/iovs.04-0694

Sherwood, D., Sponsel, W. E., Lund, B. J., Gray, W., Watson, R., Groth, S. L., . . . Reilly, M. A. (2014). Anatomical manifestations of primary blast ocular trauma observed in a postmortem porcine model. *Investigative Ophthalmology and Visual Science, 55*(2), 1124-1132. doi:10.1167/iovs.13-13295

Shim, J. H., Kim, J. Y., Park, M., Park, J., & Cho, D. W. (2011). Development of a hybrid scaffold with synthetic biomaterials and hydrogel using solid freeform fabrication technology. *Biofabrication, 3*(3), 034102. doi:10.1088/1758-5082/3/3/034102

Smith, J. E., & Garner, J. (2019). Pathophysiology of primary blast injury. *Journal of the Royal Army Medical Corps, 165*(1), 57-62. doi:10.1136/jramc-2018-001058

Sun, J., & Tan, H. (2013). Alginate-Based Biomaterials for Regenerative Medicine Applications. *Materials (Basel), 6*(4), 1285-1309. doi:10.3390/ma6041285

Tsang, V. L., & Bhatia, S. N. (2004). Three-dimensional tissue fabrication. *Adv Drug Deliv Rev, 56*(11), 1635-1647. doi:10.1016/j.addr.2004.05.001

Turner, R. C., Naser, Z. J., Logsdon, A. F., DiPasquale, K. H., Jackson, G. J., Robson, M. J., . . . Rosen, C. L. (2013). Modeling clinically relevant blast parameters based on scaling principles produces functional & histological deficits in rats. *Experimental Neurology, 248*, 520-529. doi:10.1016/j.expneurol.2013.07.008

Van Haesendonck, G., Van Rompaey, V., Gilles, A., Topsakal, V., & Van de Heyning, P. (2018). Otologic Outcomes After Blast Injury: The Brussels Bombing Experience. *Otology & Neurotology, 39*(10), 1250-1255. doi:10.1097/MAO.0000000000002012

Watson, R., Gray, W., Sponsel, W. E., Lund, B. J., Glickman, R. D., Groth, S. L., & Reilly, M. A. (2015). Simulations of Porcine Eye Exposure to Primary Blast Insult. *Transl Vis Sci Technol, 4*(4), 8. doi:10.1167/tvst.4.4.8

Weinstein-Oppenheimer, C. R., Brown, D. I., Coloma, R., Morales, P., Reyna-Jeldes, M., Diaz, M. J., . . . Acevedo, C. A. (2017). Design of a hybrid biomaterial for tissue engineering: Biopolymer-scaffold integrated with an autologous hydrogel carrying mesenchymal stem-cells. *Materials Science & Engineering. C: Materials for Biological Applications,*

79, 821-830. doi:10.1016/j.msec.2017.05.116

Wightman, J. M., & Gladish, S. L. (2001). Explosions and blast injuries. *Annals of Emergency Medicine, 37*(6), 664-678. doi:10.1067/mem.2001.114906

Xu, X., Jha, A. K., Harrington, D. A., Farach-Carson, M. C., & Jia, X. (2012). Hyaluronic Acid-Based Hydrogels: from a Natural Polysaccharide to Complex Networks. *Soft Matter, 8*(12), 3280-3294. doi:10.1039/C2SM06463D

Zhang, J., Pintar, F. A., Yoganandan, N., Gennarelli, T. A., & Son, S. F. (2009). Experimental study of blast-induced traumatic brain injury using a physical head model. *Stapp Car Crash Journal, 53*, 215-227.

Zhu, F., Wagner, C., Dal Cengio Leonardi, A., Jin, X., Vandevord, P., Chou, C., . . . King, A. I. (2012). Using a gel/plastic surrogate to study the biomechanical response of the head under air shock loading: a combined experimental and numerical investigation. *Biomechanics and Modeling in Mechanobiology, 11*(3-4), 341-353. doi:10.1007/s10237-011-0314-2